Raman excitation profiles of metallic single-walled carbon nanotubes

2010 J. Phys.: Condens. Matter 22 095302

(http://iopscience.iop.org/0953-8984/22/9/095302)

IOP Publishing Journal of Physics: Condensed Matter

J. Phys.: Condens. Matter **22** (2010) 095302 (9pp) doi:10.1088/0953-8984/22/9/095302

Raman excitation profiles of metallic single-walled carbon nanotubes

Božidar Nikolić

Faculty of Physics, University of Belgrade, PO Box 368, 11001 Belgrade, Serbia

E-mail: boza@ff.bg.ac.rs

Received 28 August 2009, in final form 20 January 2010
Published 10 February 2010
Online at stacks.iop.org/JPhysCM/22/095302

Abstract

In this work Raman excitation profiles of metallic carbon nanotubes have been calculated and thoroughly analyzed. Suppression and vanishing of the high-energy resonance is completely confirmed by our calculations. The presented results clearly show that the suppression, and finally the absence, of the resonance is caused by electron–phonon interaction and interference effects. Electron–phonon coupling for low-energy resonance is significantly larger than for high-energy resonance. Furthermore, the transition energies of those two transitions are close enough to make interference effects important. The type of interference is determined by the sign of the electron–phonon interaction matrix elements. Constructive interference makes the low-energy resonance more intensive and destructive interference destroys the high-energy resonance for most of the metallic tubes.

1. Introduction

Preparation of single-walled carbon nanotubes (SWCNTs) in solution, where they are unbundled, has opened a new direction in carbon nanotube research [1–4] and completely confirms the importance of theoretical investigation of isolated tubes. The wide variety of physical and electronic properties of carbon nanotubes is strongly dependent on the nanotube structure, i.e. on tube chiral indices (n, m) [5]. Synthesis of nanotubes with a predefined chiral index has not been achieved so far, and structural characterization and determination of the tube types presented in a sample of isolated SWCNTs becomes one of the most important tasks in the field. Unique assignment enables verification and possible revision of various theoretical models of the electronic and phonon band structure, electron–phonon interaction, Raman intensities etc. Moreover, such an assignment would allow us to characterize the tubes after their production and to control their separation.

Ever since the discovery of carbon nanotubes various experimental techniques, such as optical absorption [6], photoluminescence (PL) [2] and resonant Raman spectroscopy (RRS) [7], have been widely used for their study and characterization. Raman spectroscopy has proven to be a powerful method for characterization of SWCNTs due to the diameter and chiral angle dependence of intensity of the most intensive totally symmetric modes: the radial breathing mode (RBM) and the tangential part of the G mode, known as high-energy mode(s) (HEM).

Carbon nanotubes are quasi-one-dimensional crystals, with a large number of van Hove singularities in the electronic and phonon density of states. These singularities in electronic density of states are responsible for intense optical absorption and emission. Strong absorption in the visible light region leads to resonant or close to resonant Raman scattering. The vicinity of resonance makes the electronic system important in the Raman scattering process. Furthermore, the proximity of resonance makes the fine structure of the Raman scattering spectrum important. Taking matrix elements in the points of the Brillouin zone with the maximal transition probabilities as the usual approximation for strong resonant scattering [8] will cancel out lot of information contained in the quasi-momentum dependence of matrix elements of relevant operators.

Metallic tubes are those in which the difference in the chiral indices is divisible by three ($n - m = 0 \bmod 3$) [9, 10]. They have several interesting properties: pairs of close optical transitions [11], a Kohn anomaly [12, 13], a possible Breit–Wigner–Fano shape of G-band line [14, 15] and the vanishing of the high-energy resonance [16] are just few of the most interesting problems in the field of metallic nanotubes.

The main objective of this paper is to find a reason why the high-energy resonance is vanishing in the Raman excitation profiles (REPs). The REP should be similar to the optical conductivity in the region near resonance. Regardless of the function type, the only physical quantity which appears in the Raman tensor and not in the expression for optical conductivity

is the electron–phonon interaction matrix element. Therefore, the reason for discrepancy between the absorption spectrum and the shape of the excitation profile should come, in general, from electron–phonon interaction.

In this paper Raman excitation profiles are calculated for metallic tubes with diameters of 8–20 Å. Raman intensities are calculated using an expression derived from the third order of the time dependent perturbation theory [7], and for all calculations the full symmetry of the system is used [17]. The theoretical background, including calculation of Raman intensities in general, symmetry of SWCNTs, electronic spectra of metallic tubes and Raman excitation profiles for metallic tubes, is described in section 2. The main results are presented in section 3, including analysis of REPs, discussion of the role of electron–phonon interaction matrix elements and interference effects. The obtained results give a simple explanation for the vanishing of the high-energy resonance in Raman excitation profiles of metallic tubes.

2. Theoretical background

2.1. Calculation of Raman intensities

Raman intensity is proportional to the sum of the squares of the Raman tensor matrix elements in a light polarization vector basis [7]. For most of physical systems at low temperatures it is possible to presume that the electronic system is in the ground state. In that case there is only one initial state in the expression for Raman intensities. The same argument can be used for the final electronic state; it is the usual approximation that the final electronic state is the same as the initial one. With these assumptions the Raman intensity is described by:

$$\mathcal{I}_\mu(\omega_0) = C\left(\frac{\omega_0-\omega_\mu}{\omega_0}\right)^2 (n+1)|\mathcal{R}_\mu^{\parallel,\parallel}(\omega_0)|^2, \qquad (1)$$

where $\parallel$ denotes light polarization parallel to the tube axis, μ stands for the whole set of Raman active phonon quantum numbers, $\hbar\omega_\mu$ is phonon energy, $\hbar\omega_0$ is laser energy, n is the phonon Bose–Einstein factor, C is a constant and the Raman tensor matrix element is $\mathcal{R}_\mu^{\parallel,\parallel}(\omega_0)$. The expression for the Raman tensor matrix elements is obtained in third order time dependent perturbation theory. In the low temperature limit and in the case of single resonance it has the form [7]:

$$\mathcal{R}_\mu^{\parallel,\parallel}(\omega_0) = \sum_{i,l,k}\left[\frac{p_{il}^{\parallel\dagger}(k)\mathcal{M}_{li}^{\mu}(k)\,p_{li}^{\parallel}(k)}{((\epsilon_i(k)-\epsilon_l(k)+\hbar\omega_0-\hbar\omega_\mu)^2+\gamma_e^2)}\right.$$
$$\left.\times\frac{1}{((\epsilon_l(k)-\epsilon_i(k)-\hbar\omega_0)^2+\gamma_e^2)}\right], \qquad (2)$$

where $p_{il}^{\parallel}$ is the electron momentum component matrix element parallel to the tube axis, $\epsilon_l(k)$ is the energy of the electron state $|k,l\rangle$ and γ_e is the width of the electronic excited states. The deformation potential matrix element $\mathcal{M}_{li}^{\mu}(k)$ is actually the difference of the two matrix elements:

$$\mathcal{M}_{li}^{\mu}(k) = \mathcal{M}_{ll}^{\mu}(k) - \mathcal{M}_{ii}^{\mu}(k), \qquad (3)$$

where

$$\mathcal{M}_{ii}^{\mu}(k) = \left(\frac{\hbar}{2M\omega_\mu}\right)^{1/2} \boldsymbol{e}_\mu \cdot \frac{\partial\epsilon_i(k)}{\partial \boldsymbol{e}_\mu}. \qquad (4)$$

The normal mode (phonon) direction unit vector is $\boldsymbol{e}_\mu$, and the atom mass is M. Note that the matrix element $\mathcal{M}_{li}^{\mu}(k)$ is proportional to the derivative of the electron's transition energy with respect to the direction of displacement of the atom [18].

2.2. Symmetry of nanotubes

Carbon nanotubes are monoperiodic or quasi-one-dimensional crystals and their symmetries are line groups of the fifth (chiral tubes) or the thirteen family (achiral tubes) [17]. Symmetry of the nanotube is uniquely defined by a pair of tube chiral indices (n, m). Single-walled carbon nanotubes are single orbit systems, and it is possible to obtain the whole system by the action of group operators on a single orbit representative atom. This fact enables us to use a single carbon atom instead the entire unit cell of a nanotube for all calculations [17].

Electron and phonon energies, eigenfunctions and the required matrix elements (2) are calculated using the full symmetry of the nanotubes utilizing the modified group projector technique for induced representations [19]. A general model of the calculations is based on full symmetry of the system and uses the tight-binding approximation (FSTB), and it is incorporated in the POLSym code [20].

Electron energies and eigenfunctions are calculated using hydrogen type $2p_z$ orbitals [21] and Hamiltonian matrix elements, obtained by density functional tight-binding (DFTB) [22] calculations. Phonon energies and eigenvectors are calculated using the force constant model [23]. The great benefit of using full symmetry of the system is that all good quantum numbers are incorporated into the output of the POLSym program. The other symmetry based models [32] do not use complete symmetry of the system, and U-axis symmetry and corresponding parity is omitted (two carbon atoms are used instead of a single one).

Knowing sets of good quantum numbers for electronic and phonon states enables us to find selection rules for all possible transitions during Raman scattering. Having selection rules in advance should be also important for the time consuming calculation of electron momentum matrix elements in general. Only matrix elements for allowed transitions are calculated, others are skipped. Electron eigenfunctions (generalized Bloch functions) and selection rules are used for electron momentum matrix elements and optical conductivity calculations [21, 24]. RBM eigendirections, which are not strictly radial [23], are used for obtaining deformation potential matrix elements (4).

2.3. Metallic tubes

Metallic tubes, tubes for which the difference of the chiral indices is a multiple of 3 ($n - m = 0 \bmod 3$), have pairs of close optical transitions, with energies denoted by E_{11} and E_{22}, respectively (these energies are frequently referred to as E_{11L}^M and E_{11H}^M [25]). Pairs of close optical transitions are explained by the trigonal warping effect [11, 26]. The first two transitions are within the region of visible light, and their energies, as a function of tube diameter, are shown in figure 1. The splitting energy of the first two transitions decreases with tube diameter and depends on chiral angle. The magnitude of splitting varies from zero for armchair (n, n) nanotubes to a

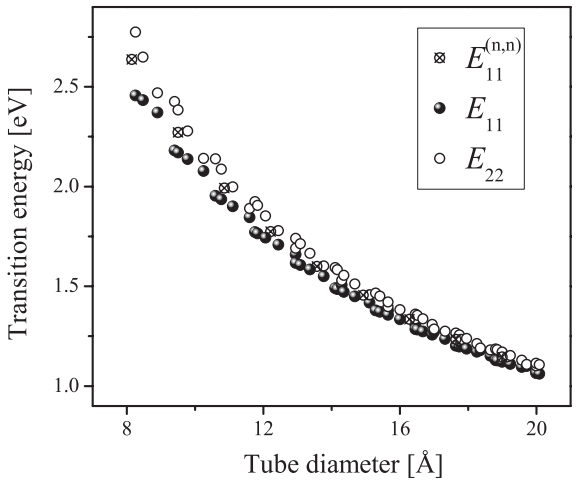

Figure 1. Energies of the first two optical transitions for metallic nanotubes (black circles stand for the low-energy optical transition and white circles for the high-energy one) and armchair tubes (crossed circles).

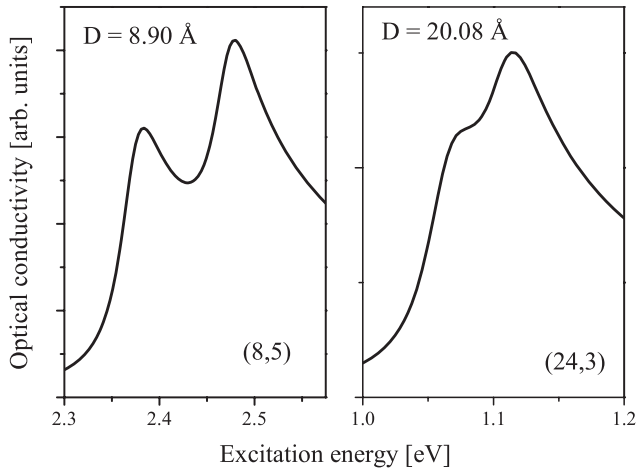

Figure 2. Optical conductivity for two metallic tubes (8, 5) and (24, 3), obtained by the FSTB model.

maximum splitting for zig-zag $(n, 0)$ tubes, as expected [25], and the magnitudes of splitting are in good agreement with previous theoretical results [27].

Results for optical conductivity obtained by the FSTB model show that the first two optical transitions are well separated in the absorption spectrum for all tubes with diameters from 8 to 20 Å. This is illustrated in figure 2, where optical conductivity is shown for two tubes, (8, 5) with diameter 8.9 Å and (24, 3) with diameter 20.1 Å. The absorption spectra of both tubes show two well defined peaks. In the case of the tube (24, 3) those two peaks are quite overlapped, but it is still possible to distinguish them.

Note that the low-energy transition intensity is lower than the high-energy one. This is opposite to the recent experimental results obtained for individual SWCNTs [28]. The discrepancy could arise from the simplicity of the applied tight-binding model which neglects many-body effects, which should be important for intensities and peak shapes in absorption spectra as it is theoretically shown in [29].

2.4. Raman intensities for SWCNTs

The Raman intensity for a particular mode is a smooth function of laser energy, called the Raman excitation profile (REP). The excitation profile should be similar to the optical absorption spectrum. Electronic transition energies within the visible light interval should make strong resonant scattering. Because of the strong resonance, excitation profiles should have local maxima at almost the same positions as the optical absorption spectrum. Detailed analysis of the REPs is a good way to find a lot of important details about possible unique characterization of SWCNTs [25, 30–35].

In the case of resonant or close to resonant Raman scattering only two processes are dominant [7]. Two terms in equation (2) are related to those two processes. The contribution of other four processes is negligible. Because of the intensive light absorption of SWCNTs such an approximation seems to be good for all laser energies from the entire visible light region. Furthermore, all matrix elements and electron energies in (2) are functions of quasi-momentum k. In the strong resonance scattering limit only dominant terms can be used—matrix elements and electron energies in the points of Brillouin zone with the maximal transition probabilities [7] or effective mass approximation for electronic bands [32]. On the other hand, if precise estimation of Raman intensities is important for energies which are close to the resonance as well, retaining quasi-momentum dependence of matrix elements and electron energies obtained as eigenvalues of Hamiltonian should be important. Summing in (2) is performed over all electronic states around the Fermi level with transition energies less than 3 eV.

According to the Khan and Allen theorem [36] deformation potential is a good approximation for electron–phonon interaction only in the points of the Brillouin zone with maximal transition probability. For totally symmetric modes deformed configurations have the same symmetry as the initial one and therefore there is no need for correction terms: the Brillouin zone remains the same during totally symmetric deformation, the transition energy derivative is used and changing of the Fermi level energy is irrelevant [18]. Moreover, some kind of continuity of the matrix elements must exist, and the matrix elements, as a functions of quasi-momentum, obtained by presented model should be a good approximation around resonance as well.

Excitonic effects are not included in Raman intensity calculations because it is shown that they are much smaller than in the semiconducting case [34, 29] and they do not contribute to the qualitative picture of resonant Raman scattering in metallic tubes. Excitonic corrections result in a shift of transition energies [27].

3. Results

3.1. REPs of metallic tubes

Excitation profiles of metallic tubes have quite interesting features. Comparing excitation profiles shown in figure 3,

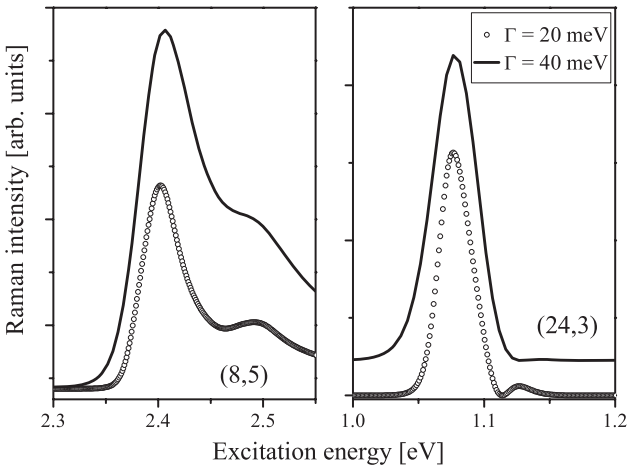

Figure 3. Raman excitation profiles for two metallic tubes (8, 5) and (24, 3). Solid and dotted lines are for $\gamma_e = 40$ meV and $\gamma_e = 20$ meV, respectively. Note that for the (24, 3) tube both excitation profiles start with zero intensity, and they are separated just for clarity.

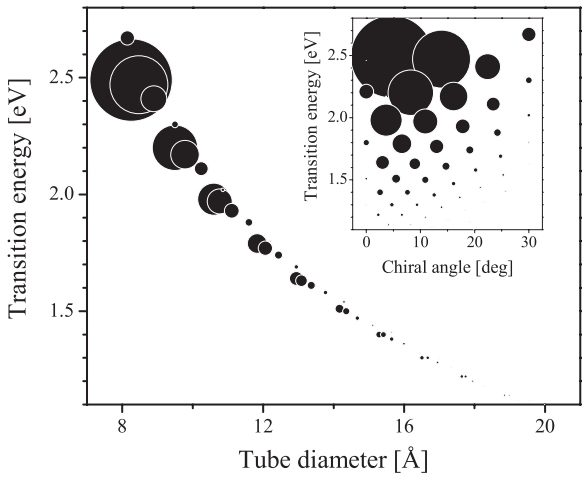

Figure 4. Resonant intensities of metallic tubes as a function of the diameter (main panel), chiral angle (inset) and transition energies. The size of the symbols is scaled with intensity.

for parallel polarization, with optical conductivity, figure 2, it is obvious that the high-energy resonance is strongly suppressed for tube (8, 5) and completely vanishes for tube (24, 3). Moreover, even for tube (8, 5), if excitation profile is calculated for more realistic and slightly larger values of the electronic bandwidth parameter, γ_e, high-energy resonance will disappear. This result completely confirms the well known experimental fact that the high-energy resonance peak vanishes in the excitation profile for the radial breathing mode [16, 37, 38].

Vanishing of the high-energy resonance is a general feature of all metallic tubes [16, 39]. Excitation profiles are calculated and analyzed for tubes with diameters within the interval from 8 to 20 Å. Resonant intensities for all these tubes are shown in figure 4. Intensities are plotted as a function of diameter, chiral angle and transition energy in a modified form of Kataura plot [6, 30]. Transition energy dependence on the diameter and chiral angle is shown in these figures, and symbol size is scaled with the intensity. Diameter dependence of the resonant intensities is given in the main figure and in the inset the chiral angle dependence is shown.

Because of the rapidly decreasing intensities, suppression of the high-energy resonance is presented in a clearer form in figure 5, where the energy interval is divided into three regions, and the position of the vanished peaks is denoted by white circles. It is clear that the high-energy resonance vanishes, or, in just a few cases, is strongly suppressed.

Resonant intensities decrease rapidly with increasing tube diameter. Moreover, the diameter dependence shows branch structure as expected [30]. A branch is formed of tubes with constant $2n + m$, in the increasing order of the chiral angle. Within each branch intensity decreases, in general. The absolute intensity maximum for all branches is between 5° and 15°, which is completely verified by experimental results [31, 40].

To exclude numerical resolution as a possible source of vanishing of the high-energy resonance, REPs were also calculated for $\gamma_e = 20$ meV, with qualitatively the same result.

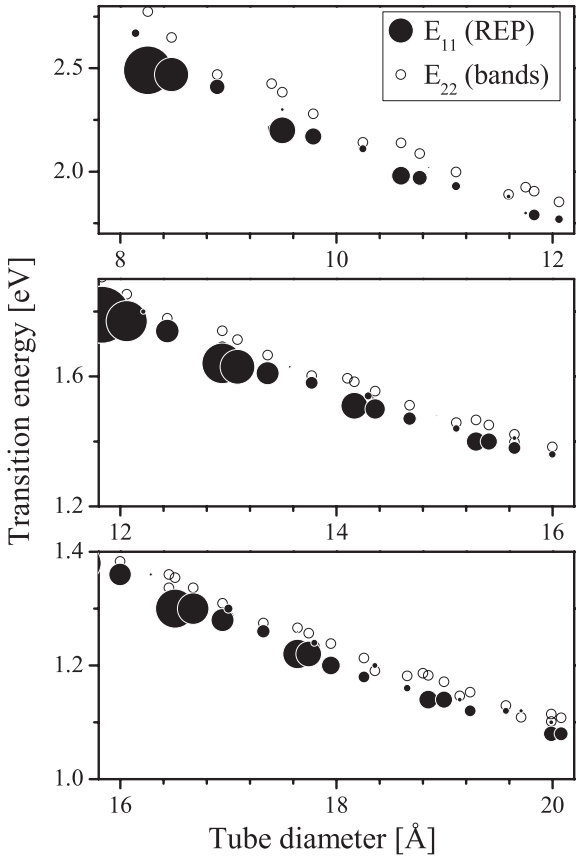

Figure 5. Resonant intensities of metallic tubes (black circles). White circles represent the energies, obtained from electronic bands, where the high-energy resonance should occur.

3.2. Electron–phonon interaction

Resonant intensity is predominantly defined by the magnitude of the Raman tensor matrix element (2) at the point of the Brillouin zone where transition probability has its maximum. The intensity ratio for the first two resonances in excitation

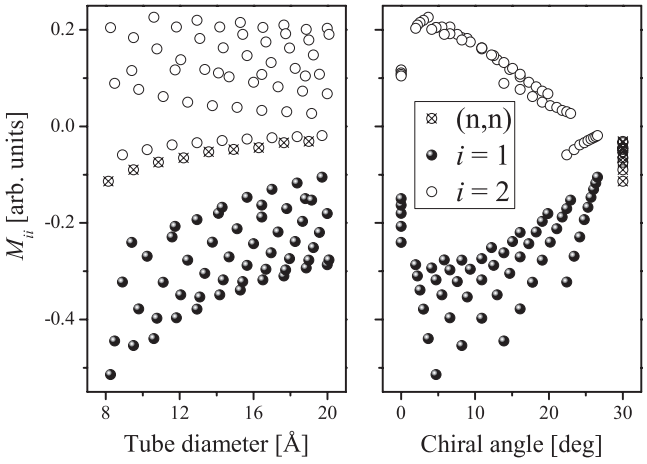

Figure 6. Electron–phonon matrix elements for the first two optical transitions. Dependence on diameter is given in the left panel, and on chiral angle in the right one.

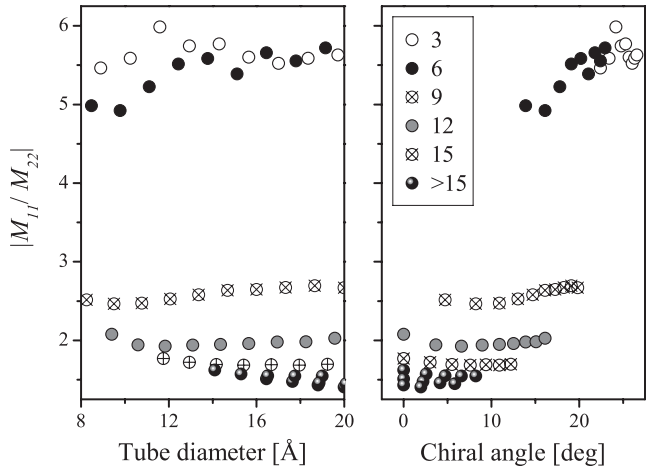

Figure 7. Electron–phonon matrix elements ratio, M_{11}/M_{22}, as a function of tube diameter (left panel) and chiral angle (right panel). Tubes within the same $n - m$ class are represented by the same symbols.

profiles is determined by the magnitude of the electron–phonon interaction matrix elements in those points [30, 33, 41].

The fact that SWCNTs are single orbit systems makes calculation of deformation potential matrix elements fairly easy. The use of total symmetry of the system makes it possible to move one atom (orbit representative atom) along the displacement direction, and then acting by group elements reconstructs the whole tube. Then, the electronic spectrum is found for the deformed tube. Electronic spectra for few displaced configurations enable one to find the numerical derivative of electronic energy with respect to displacement magnitude. Note that because total symmetry of the system has been used there is no sum over atoms in the unit cell in (4).

Matrix elements of the electron–phonon interaction, in the points of the Brillouin zone with maximal transition probability, for all referred metallic tubes are shown in figure 6. Clear family patterns can be observed with the descent of the matrix elements within the same tubes' family, just as shown in other theoretical results [41]. One tubes' family comprises the tubes with the same difference of the tube indices, $n - m = \text{const}$. Matrix elements corresponding to the first two transitions have opposite signs [39], except for the tubes with large chiral angle (with $n-m = 3$, figure 6) (this is in complete agreement with the results obtained using another symmetry based model [32] and slightly different from those in [33] where the family $n - m = 6$ has the same property). The second important point is that matrix elements for the low-energy transition have larger values than those for the high-energy one, as shown in [41]. To make this clearer, figure 7 shows the M_{11}/M_{22} ratio as a function of diameter and chiral angle. Metallic tubes with the largest chiral angle ($n - m = 3$, $n - m = 6$) have the greatest matrix elements ratio, which completely matches results from previous calculations [25]. As the chiral angle goes down the matrix elements ratio increases, but it is always greater than 1. It is interesting that in the family of tubes with the same difference in chiral indices, $n - m = \text{const}$, the matrix elements ratio is almost constant. For example, for $n - m = 9$ $M_{11}/M_{22} \approx 2.5$, which is the same as in [32] where the same ratio is found for a (16, 7) tube. Furthermore, stronger electron–phonon coupling for the low-energy resonance, for all metallic tubes, is verified experimentally [42] and theoretically [32].

Note that for tubes with a large chiral angle (closest to the armchair ones) where the matrix elements ratio is greatest (figure 7), the high-energy resonant peak is visible (well defined shoulder, figure 3). Analogously, for tube with a small chiral angle the high-energy resonant peak is unobservable, while the matrix element ratio is significantly less than for $n - m = 3$ tubes. According to the matrix elements ratio, the high-energy resonant peak should be observable for tubes with small chiral angles, and as the chiral angle increases, the intensity of the high-energy resonance should fade away. But this is not happening, in general.

3.3. Interference effects

If two resonant transitions are very close then some interference effects should occur. The splitting energy of the first two optical transitions of metallic tubes is mostly well below 0.1 eV (figure 1). In that case, excitation profiles of metallic tubes should have a typical interference shape. Interference could be constructive or destructive, depending on the sign of the matrix elements for the neighboring transitions (see appendix). The expression for Raman intensity, (2), shows that if two neighboring transition matrix elements have the same sign then, if they are very close, some constructive interference will happen, although if their signs are opposite than destructive interference will occur. In the case when light polarization is parallel to the tube axis, the sign of matrix element's product is defined by sign of the electron–phonon matrix element. The existence of interference indicates that besides the magnitude of the electron–phonon interaction matrix elements, their signs are also important. Signs of the relevant matrix elements will determine which type of interference will occur in the excitation profile.

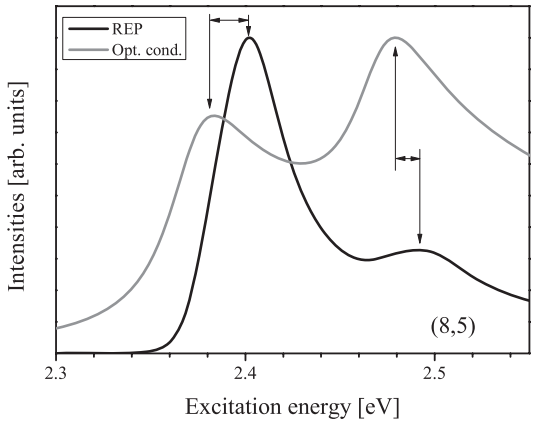

Figure 8. Excitation profile compared to optical conductivity for an (8, 5) tube. Both intensities are normalized to unity.

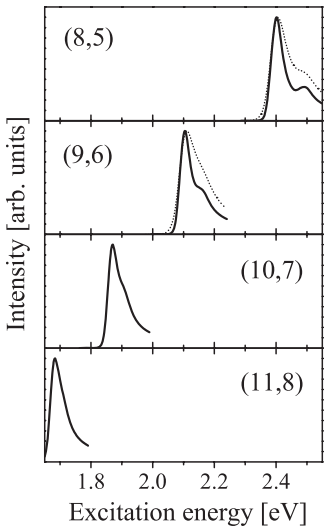

Figure 9. Excitation profiles for $n - m = 3$ tubes. Profiles calculated using $\gamma_e = 20$ meV are denoted by a solid line. Dotted lines represent profiles for $\gamma_e = 40$ meV.

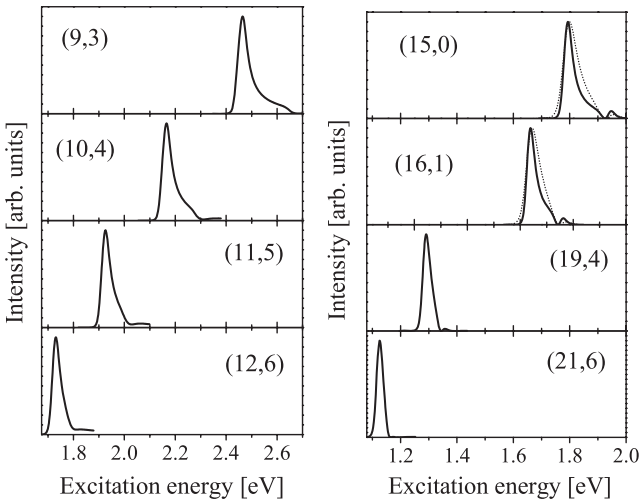

Figure 10. Excitation profiles for $n - m = 6$ (left panel) and $n - m = 15$ (right panel) tubes.

Furthermore, resonant intensities are completely determined by the magnitude of the matrix elements in the points of the Brillouin zone with maximal transition probability. But for the fine analysis of the shape of excitation profiles it should be important to know intensities between resonances as well. All matrix elements appearing in (2) are obtained as functions of quasi-momentum, as explained in section 2.4, and they are used for the calculation of intensities.

The excitation profile for the (8, 5) tube has a typical constructive interference shape (figure 3). Matrix elements of $n - m = 3$ tubes have the same sign, and interference will be constructive. The effect of interference is illustrated more clearly in figure 8, where REP is compared to optical conductivity for an (8, 5) tube. Besides suppression of the high-energy resonance, the maxima of the REP are shifted to higher energies, and the energy shift is slightly above half of the RBM phonon energy [7]. The resonant energy is shifted more for low-energy transitions than for high-energy ones, and the interference effect is typically constructive as well. Moreover, constructive interference will increase the low-energy resonant intensity. The constructive interference shape of the excitation profile for tubes within the $n - m = 3$ family is verified experimentally [35], and in the general case [27]. Constructive interference is verified indirectly, as well, by discovering that the strongest resonance for metallic tubes is for those with chiral angles closest to the armchair ones ($n - m = 3$) [38]. Increase in the resonant intensity is caused by two close resonances, but it should be a consequence of constructive resonance as well.

The general behavior of the excitation profiles for $n - m = 3$ family tubes is illustrated in figure 9, where REPs for four tubes are shown. The high-energy resonance can be observed only for the narrowest tube (8, 5) (dotted line). As diameter increases within the $n-m = 3$ family the high-energy resonance will be covered by the low-energy one.

For all other tube families (figure 10) the sign of matrix elements is opposite and destructive interference will destroy high-energy resonance. Destructive interference and vanishing of the high-energy resonance is also confirmed experimentally [42] and theoretically [33].

According to the presented arguments, constructive interference will rise up the high-energy resonance peak, for narrow $n - m = 3$ tubes, regardless of the matrix elements ratio. For all other tubes destructive interference appears, and only for narrow tubes with a large chiral angle could a second resonance be observed because transition energies are sufficiently separated, as measured recently [43]. Further, within the same family of metallic SWNTs interference becomes more important as chiral angle increases, which is in good agreement with previous results [25, 39]. It is shown that constructive interference is quite a general feature for the entire $n - m = 3$ family and interference will be destructive for all other families, which is slightly different than in [25].

It is worth noting that the splitting energy of the first two optical transitions for an (8, 5) tube is $\Delta\epsilon \sim 1$ eV, which is 2.5 times larger than electronic bandwidth, $\gamma_e = 40$ meV, used in this calculation, and constructive interference

is still observable. According to presented results the interference region should be much wider than previously estimated [32]. Constructive interference will be observable, at least theoretically, up to $\Delta\epsilon = 3\gamma_e$. Constructive interference effects appear in two ways, through increasing of both resonant intensities and resonances becoming closer than in the noninterference case.

Dependence of the Raman matrix elements on quasi-momentum, (2), could be one of the reasons for widening of the interference region. Obtained excitation profiles are not symmetric, as in the case when the strong resonance approximation is applied, where REPs are a superposition of two Lorentzians. Dependence on quasi-momentum of the matrix elements makes profiles slightly nonsymmetric, as can be seen in figures 9 and 10. Nonsymmetric profiles have a tails for energies above resonance and that could be a reason for widening of the interference region.

Finally, experimental results look inconsistent. Some results show clear high-energy resonance [35, 42] and others do not [38]. As it can be seen from our results, the existence of high-energy resonance is strongly dependent on the value of the electronic bandwidth, γ_e. Besides, γ_e strongly depends on the environment of isolated tubes. Furthermore, it is not clear how electron correlation effects affect the results. According to results for absorption spectra [29], absorption intensities are strongly dependent on correlation effects, and they should be important for Raman intensities as well. A simple approximation like tight-binding, used here, should give a good qualitative picture and simple explanation of the physical reasons for suppressing and vanishing of the high-energy resonance, for all metallic nanotubes.

4. Conclusion

In conclusion, Raman excitation profiles are calculated for metallic carbon nanotubes in the diameter range from 8 to 20 Å and for transition energies up to 3 eV, within the framework of the theoretical model based on full symmetry of SWCNTs and the third order perturbation theory, the dipole approximation for optical transitions and the deformation potential approximation for electron–phonon interaction. A branch structure of resonant intensities in a modified form of the Kataura plot is evident. Branches are formed by tubes with constant $2n + m$. Strong suppression of the high-energy resonance is observed and it is confirmed as a general feature of metallic tubes.

The presented results clearly explain the vanishing of the high-energy resonance. At first, electron–phonon coupling is stronger for the low-energy electronic transition than for the high-energy one. Corresponding matrix elements are from 2 to 6 times larger for the low-energy transition. Besides, electron–phonon interaction matrix elements show obvious family behavior. Signs of the matrix elements and matrix elements ratio are the same for tubes within the same $n - m$ family. Besides, the closeness of these two transition energies makes interference effects significant. For the NTs within the $n - m = 3$ family the matrix elements of both transitions are of the same sign and constructive interference will enlarge resonant intensity. For all other families matrix elements are of the opposite sign, and destructive interference makes the high-energy resonant peak unobservable. It is shown that the interference region is about three times wider than previously estimated. Furthermore, the type of interference (constructive or destructive) depends only on the sign of the corresponding electron–phonon interaction matrix elements. Finally, interplay of the electron–phonon matrix elements ratio and type of interference, which is strictly a $n - m$ family property, is responsible for vanishing of the high-energy resonance.

Acknowledgments

The author would like to thank G Seifert for DFTB input data, M Damnjanović and I Milošević for guidance and J Maultzsch for helpful and fruitful discussion. This work is supported by the Serbian Ministry of Science (project ON141017) and the European Union (project FP6 INCO-WBC 026303).

Appendix. Interference effects in Raman excitation profiles

For emphasizing important facts about interference effect, and to make them as simple as possible, it is good to simplify the expression for Raman intensity (without losing any important qualitative information). The expression for Raman tensor matrix elements can be rewritten as

$$\mathcal{R}_\mu^{\parallel,\parallel}(\omega_0) = \sum_{i,l,k} R_{ilk}^\mu(\omega_0), \tag{A.1}$$

where

$$R_{ilk}^\mu(\omega_0) = \frac{J_{il}^\mu(k)}{((\epsilon_i(k) - \epsilon_l(k) + \hbar\omega_0 - \hbar\omega_\mu)^2 + \gamma_e^2)} \times \frac{1}{((\epsilon_l(k) - \epsilon_i(k) - \hbar\omega_0)^2 + \gamma_e^2)}. \tag{A.2}$$

$J_{il}^\mu(k)$ is a product of matrix elements (2):

$$J_{il}^\mu(k) = p_{il}^{\parallel\dagger}(k)\mathcal{M}_{li}^\mu(k)p_{li}^\parallel(k) = |p_{il}^\parallel(k)|^2\mathcal{M}_{li}^\mu(k). \tag{A.3}$$

In the strong resonance case terms including resonant transition dominate in the sum. The sum (A.1) can be restricted to electronic states corresponding to resonant transitions. The sum over quasi-momentum can be reduced to a sum over k-points with maximal transition probability:

$$\sum_{i,l,k} R_{ilk}^\mu(\omega_0) \approx \sum_{i,l}{}' R_{il}^\mu(\omega_0, \tilde{k}_{il}), \tag{A.4}$$

where the prime in the sum denotes summing over resonant states, and $\tilde{k}_{il}$ is a k-point where the transition probability has its maximum for the $i \to l$ transition.

Let us suppose that we have a system with two optical transitions in some interval of excitation energies. Let those two transitions be from initial state i to n, and from j to m.

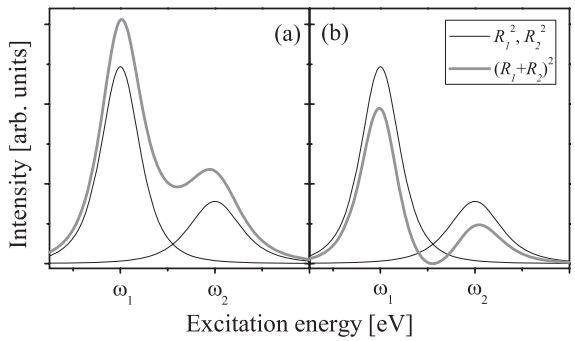

Figure A.1. Constructive interference (a) and destructive interference (b). Black thin lines denote intensities of particular resonant transitions, and the thick gray line represents cumulative intensity.

Then the whole sum in (A.4) could be approximated by the sum of two resonant terms:

$$\sum_{i,l}{}' R^{\mu}_{il}(\omega_0, \tilde{k}_{il}) \approx R^{\mu}_{in}(\omega_0, \tilde{k}_{in}) + R^{\mu}_{jn}(\omega_0, \tilde{k}_{jn}). \qquad \text{(A.5)}$$

Furthermore, let the energy of the first electronic transition be denoted by $\hbar\omega_1$, and of the second one by $\hbar\omega_2$, and let the matrix elements be $R^{\mu}_{in}(\omega_0, \tilde{k}_{in}) = R_1$ and $R^{\mu}_{jm}(\omega_0, \tilde{k}_{jm}) = R_2$ for simplicity, then

$$\sum_{i,l}{}' R^{\mu}_{il}(\omega_0, \tilde{k}_{il}) \approx R_1 + R_2. \qquad \text{(A.6)}$$

R_i $(i = 1, 2)$ is the product of three matrix elements and two bell-type functions (Lorentzians), (A.2) and (A.3). The centers of these two functions are shifted by phonon energy $\hbar\omega_\mu$, and their maxima correspond to incoming and outgoing resonance. Energies of RBM for metallic tubes are less than 20 meV, which is significantly below the transition energies shown in figure 1, and less than realistic values of electronic bandwidth, γ_e. In that case two maxima for such a a function are not observable. Finally, for small phonon energies, such as the energy of RBM, the product of two bell-type functions (A.2) is effectively a single bell-like function with a single maximum. In the case of two resonant transitions the excitation profile can be treated, roughly, as a combination of two Lorentzians:

$$I_\mu(\omega_0) \propto (R_1 + R_2)^2. \qquad \text{(A.7)}$$

The sign of R_i $(i = 1, 2)$ terms is defined by the sign of $J^{\mu}_{il}(k)$, and it depends only on the sign of electron–phonon interaction matrix elements; all other quantities are positive (A.2). If resonant energies ω_1 and ω_2 are close enough, then Lorentzians R_1 and R_2 are significantly overlapped. In such a case interference should emerge. Depending on the signs of R_1 and R_2 two types of interference could happen. If both terms are of the same sign then constructive interference will occur, as shown in figure A.1(a). Due to constructive interference the intensities of both resonances are increased compared to the intensity of any isolated one. Furthermore, maximal intensities look as if they are slightly attracted to each other, figure A.1, due to interference as well. If matrix elements have opposite signs then destructive interference will take place, as shown in figure A.1(b). The resonant intensities are then lowered due to interference and the maximal intensities slightly repel each other.

All previous conclusions are valid even for a more precise expression for Raman intensities (2), as well. Observable separation of the incoming and outgoing resonance for a single resonant transition does not change the qualitative picture of the possible type of interference.

References

[1] O'Connell M J *et al* 2002 *Science* **297** 593
[2] Bachilo S M, Strano M S, Kittrell C, Hauge R H, Smalley R E and Weisman R B 2002 *Science* **298** 2361
[3] Lefebvre J, Homma Y and Finnie P 2003 *Phys. Rev. Lett.* **90** 217401
[4] Lebedkin S, Hennrich F, Skipa T and Kappes M M 2003 *J. Phys. Chem.* B **107** 1949
[5] Reich S, Thomsen C and Maultzsch J 2004 *Carbon Nanotubes (Basic Concepts and Physical Properties)* (Berlin: Wiley–VCH)
[6] Kataura H, Kumazawa Y, Maniwa Y, Umezu I, Suzuki S, Ohtsuka Y and Achiba Y 1999 *Synth. Met.* **103** 2555–8
[7] Thomsen C and Reich S 2006 Raman scattering in carbon nanotubes *Light Scattering in Solids IX* (*Topics in Applied Physics* vol XX) ed M Cardona and R Merlin (New York: Springer)
[8] Martin R M and Falicov L M 1975 Resonant Raman scattering *Light Scattering in Solids I Introductory Concepts* (*Topics in Applied Physics* vol VIII) ed M Cardona (Berlin: Springer) p 79
[9] Hamada N, Sawada S and Oshiyama A 1992 *Phys. Rev. Lett.* **68** 1579
[10] Saito R, Fujita M, Dresselhaus G and Dresselhaus M S 1992 *Phys. Rev.* B **46** 1804–11
[11] Saito R, Dresselhaus G and Dresselhaus M S 2000 *Phys. Rev.* B **61** 2981–90
[12] Maultzsch J, Reich S, Thomsen C, Requardt H and Ordejón P 2004 *Phys. Rev. Lett.* **92** 075 501
[13] Piscanec S, Lazzeri M, Mauri F, Ferrari A C and Robertson J 2004 *Phys. Rev. Lett.* **93** 185503
[14] Brown S D M, Jorio A, Corio P, Dresselhaus M S, Dresselhaus G, Saito R and Kneipp K 2001 *Phys. Rev.* B **63** 155414
[15] Paillet M, Poncharal Ph, Zahab A, Sauvajol J L, Meyer J C and Roth S 2005 *Phys. Rev. Lett.* **94** 237401
[16] Strano M S, Doorn S, Haroz E H, Kittrell C, Hauge R H and Smalley R E 2004 *Nano Lett.* **3** 1091
[17] Damnjanović M, Milošević I, Vuković T and Sredanović R 1999 *Phys. Rev.* B **60** 2728–39
[18] Machón M, Reich S, Telg H, Maultzsch J, Ordejón P and Thomsen C 2005 *Phys. Rev.* B **71** 35416
[19] Damnjanović M, Milošević I, Vuković T and Marinković T 2004 *J. Phys. A: Math. Gen.* **37** 4059–68
[20] Milošević I, Damjanović A and Damnjanović M 1996 Symmetry oriented computer research of polymers: program polsym and DNA *Quantum Mechanical Simulation Methods in Studying Biological Systems* les editions de physique edition, ed D Bicout and M Field (Berlin: Springer) chapter XIV, pp 295–311 (Les Houches Workshop, May 1995)
[21] Milošević I, Vuković T, Dmitrović S and Damnjanović M 2003 *Phys. Rev.* B **67** 165418
[22] Porezag D, Frauenheim Th, Köhler Th, Seifert G and Kaschner R 1995 *Phys. Rev.* B **51** 12947
[23] Dobardžić E, Milošević I, Nikolić B, Vuković T and Damnjanović M 2003 *Phys. Rev.* B **68** 45408
[24] Milošević I, Nikolić B and Damnjanović M 2004 *Phys. Rev.* B **69** 113408

[25] Jiang J, Saito R, Grüneis A, Chou S G, Samsonidze Ge G, Jorio A, Dresselhaus G and Dresselhaus M S 2005 *Phys. Rev.* B **71** 205420
[26] Reich S and Thomsen C 2000 *Phys. Rev.* B **62** 4273–76
[27] Souza Filho A G, Kobayashi N, Jiang J, Grüneis A, Saito R, Cronin S B, Mendes Filho J, Samsonidze Ge G, Dresselhaus G and Dresselhaus M S 2005 *Phys. Rev. Lett.* **95** 217403
[28] Sfeir M Y *et al* 2006 *Science* **312** 554–6
[29] Deslippe J, Spataru C D, Prendergast D and Louie S G 2007 *Nano Lett.* **7** 1626–30
[30] Maultzsch J, Telg H, Reich S and Thomsen C 2005 *Phys. Rev.* B **72** 205438
[31] Telg H, Maultzsch J, Reich S, Hennrich F and Thomsen C 2004 *Phys. Rev. Lett.* **93** 177401
[32] Popov V N and Lambin P 2006 *Phys. Rev.* B **73** 165425
[33] Popov V N, Henrard L and Lambin P 2005 *Phys. Rev.* B **72** 035436
[34] Jorio A *et al* 2005 *Phys. Rev.* B **71** 075401
[35] Canonico M, Adams G B, Poweleit C, Menéndez J, Page J B, Harris G, van der Meulen H P, Calleja J M and Rubio J 2002 *Phys. Rev.* B **65** 201402(R)
[36] Khan F S and Allen P B 1984 *Phys. Rev.* B **29** 3341–49
[37] Fantini C, Jorio A, Souza M, Strano M S, Dresselhaus M S and Pimenta M A 2004 *Phys. Rev. Lett.* **93** 147406
[38] Jorio A, Saito R, Fantini C, Hafner J H, Lieber C M, Hunter M, McClure T, Dresselhaus G and Dresselhaus M S 2001 *Phys. Rev. Lett.* **86** 1118
[39] Bussi G, Menédez J, Ren J, Canonico M and Molinari E 2005 *Phys. Rev.* B **71** 041404
[40] Jorio A *et al* 2005 *Phys. Rev.* B **72** 075207
[41] Jiang J, Saito R, Samsonidze Ge G, Chou S G, Jorio A, Dresselhaus G and Dresselhaus M S 2005 *Phys. Rev.* B **72** 235408
[42] Son H, Reina A, Samsonidze Ge G, Saito R, Jorio A, Dresselhaus M S and Kong J 2005 *Phys. Rev.* B **74** 073406
[43] Jungen A, Popov V N, Stampfer C, Durrer L, Stoll S and Hierold C 2007 *Phys. Rev.* B **75** 041405(R)